Multifunctional Plasmonic Shell–Magnetic Core Nanoparticles for Targeted Diagnostics, Isolation, and Photothermal Destruction of Tumor Cells

Zhen Fan, Melanie Shelton, Anant Kumar Singh, Dulal Senapati, Sadia Afrin Khan, and Paresh Chandra Ray*

Department of Chemistry, Jackson State University, Jackson, Mississippi 39217, United States

ABSTRACT

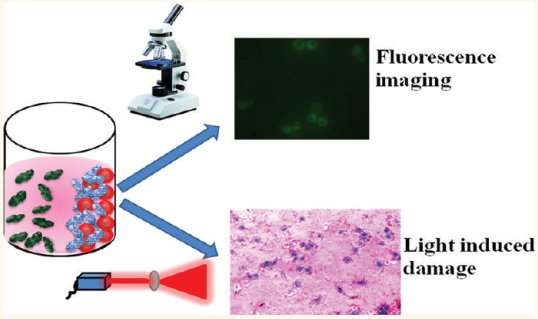

Cancer is the greatest challenge in human healthcare today. Cancer causes 7.6 million deaths and economic losses of around 1 trillion dollars every year. Early diagnosis and effective treatment of cancer are crucial for saving lives. Driven by these needs, we report the development of a multifunctional plasmonic shell–magnetic core nanotechnology-driven approach for the targeted diagnosis, isolation, and photothermal destruction of cancer cells. Experimental data show that aptamer-conjugated plasmonic/magnetic nanoparticles can be used for targeted imaging and magnetic separation of a particular kind of cell from a mixture of different cancer cells. A targeted photothermal experiment using 670 nm light at 2.5 W/cm^2 for 10 min resulted selective irreparable cellular damage to most of the cancer cells. We also showed that the aptamer-conjugated magnetic/plasmonic nanoparticle-based photothermal destruction of cancer cells is highly selective. We discuss the possible mechanism and operating principle for the targeted imaging, separation, and photothermal destruction using magnetic/plasmonic nanotechnology.

KEYWORDS: plasmonic shell–magnetic core nanoparticle · cancer cell isolation · targeted cancer imaging · photothermal destruction

Cancer presents a great challenge to public healthcare and the global economy because mortality and morbidity due to cancer cost nearly 1 trillion dollars a year.[1−7] Moreover, cancer accounts for 13% of all deaths worldwide (2007 data); this trend is projected to continue rising with an estimated 12 million deaths per year by 2030.[1−6] As a result, the early detection and effective treatment of cancer will save not only millions of lives worldwide but billions of dollars each year, as well. Current treatments based on surgery, radiation therapy, and chemotherapy are often associated with severe side effects.[1−7] Therefore, new approaches to treat cancer that do not rely on traditional therapeutic regimes are very important.[5−25] Driven by this need, we report a multifunctional plasmonic shell–magnetic core nanotechnology-driven approach for targeted early detection, isolation, and photothermal destruction of cancer cells. The elegant multifunctional materials in biological systems inspire scientists to design analogous hierarchical structures with multifunctional capabilities characterized by surface-sensitive functions such as sensing, separation, and selective therapy.[15−20] Multifunctional material development is a critical multidisciplinary and interdisciplinary field of the 21st century for biomedical imaging and therapeutic action.[8−30]

As reported during the past decade, plasmonic gold nanoparticles and super-paramagnetic iron oxide nanoparticles are highly promising therapeutic agents.[8−64] Upon successful trials, they may be used as drugs in photothermal therapy. Gold nanoparticles of different sizes and shapes with optical properties tunable in the near-infrared (NIR) region are very useful for cancer imaging as a result of their high transmission rate through biological tissues.[8−17,45−60] On the other hand, iron oxide magnetic nanoparticles have been used as contrast agents in magnetic resonance imaging (MRI) and biological separation.[18−40] In addition to their biocompatibility, lack of toxicity, and ability to generate high temperatures at a desired site, perhaps the greatest promise of plasmonic gold nanotechnology medicine will be its use in the early detection

* Address correspondence to paresh.c.ray@jsums.edu.

Received for review July 24, 2011 and accepted January 25, 2012.

Published online January 25, 2012
10.1021/nn2045246

and therapeutic challenges of cancer.[8−17,45−64] Similarly, magnetic nanoparticles can also mediate localized hyperthermia effects in the presence of a strong magnetic field.[18−40] As a result, the integration of magnetic and plasmonic functions into a single platform such as a magnetic core with plasmonic shell would be hugely beneficial for cancer nanomedicine. Plasmonic gold coating on magnetic nanoparticles is very useful for stabilizing high-magnetic-moment nanoparticles in corrosive biological conditions. It will also allow easy bioconjugation through the well-understood chemistry of Au−S.[15−20] Recent reports[65−69] indicate that, in the early stage of cancer, the concentration of cancerous cell is around 0.004% of all white cells in blood. As a result, detecting these cells without separation is challenging.[65−69] Also, there are high demands to be able to detect and analyze rare cells like circulating endothelial cells and circulating tumor cells from a complex mixture of heterogeneous cells in blood samples in "personalized medicine". Therefore, in clinical settings, we need a material possessing abilities for selective sensing as well as cell separation.[65−69] It was recently reported that selective photothermal destruction from mixed cells is somehow limited.[69] Normal cells may also be killed nonspecifically as a result of increased temperature in the whole mixture of cell suspension upon light exposure. For this purpose, aptamer/antibody-conjugated core/shell composite plasmonic−magnetic nanoparticles will be extremely useful for highly sensitive plasmonic sensing, magnetic cell separation, and selective photothermal killing.

To demonstrate the capability of magnetic core−plasmonic shell nanoparticles for selective cancer cell imaging, isolation, and photothermal destruction, we used four different cell lines in the current experiment. We used the well-characterized SK-BR-3 human breast cancer cell line, which overexpresses the epithermal growth factor receptor HER2/c-erb-2/Neu (HER2) on the cell surface. We used the HER2-negative human breast cancer MDA-MB cell line. We also used human prostate cancer cell line LNCaP, which overexpresses prostate-specific membrane antigen (PSMA). Lastly, we used human skin HaCaT keratinocytes, a normal skin cell line. Using an enzyme-linked immunosorbent assay kit, we found that the amount of HER2 in SK-BR-3 cells was 6.3×10^6/cell but only 1.1×10^3/cell in the case of MDA-MB breast cancer cells. No HER2 was found in HaCaT or LNCaP cells. Since the S6 aptamer is known to exhibit highly specific targeting for the SK-BR-3 cell line *via* HER2,[13] we used S6 aptamer-conjugated iron oxide core−gold shell magnetic/plasmonic nanoparticle for the specific targeting of SK-BR-3 cells.

RESULTS AND DISCUSSION

For the magnetic separation of cancer cells followed by fluorescence imaging, we first modified the magnetic/plasmonic nanoparticle surface with a cancer-targeting aptamer. As shown in Figure 1, Cy3-modified

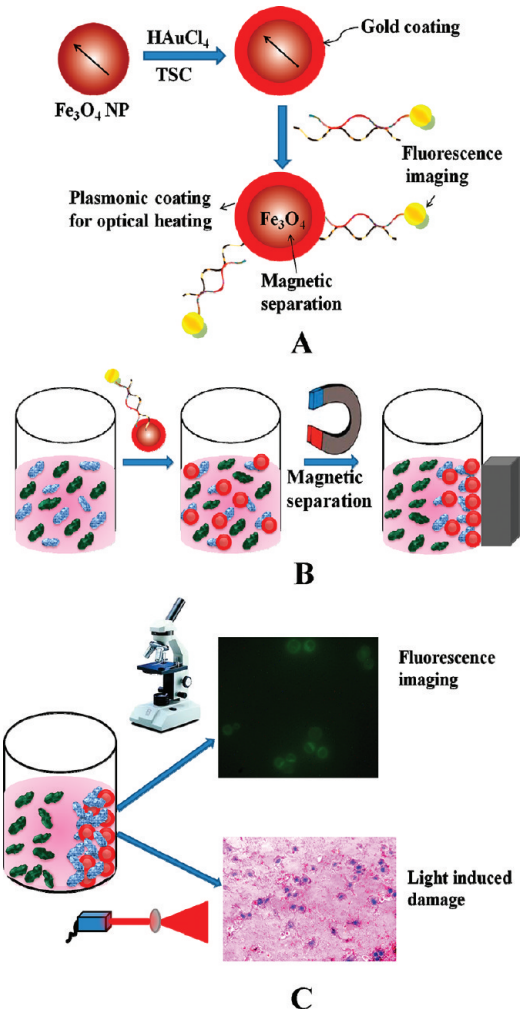

Figure 1. (A) Schematic representation showing the synthesis of S6 aptamer-conjugated multifunctional magnetic core−gold shell nanoparticles. (B) Schematic representation showing the separation of specific cancer cells using S6 aptamer-conjugated plasmonic/magnetic nanoparticles. (C) Schematic representation showing the selective fluorescence imaging and targeted photothermal destruction of specific cancer cells.

S6 aptamers were attached to magnetic/plasmonic nanoparticles through −SH linkage. Also, as shown in Figure 1, in multifunctional nanoparticles, gold plasmonic shells were used as both a photothermal agent and a nano platform. The plasmonic shell was functionalized with aptamer modified with Cy3 for (a) specific breast cancer cell recognition *via* the aptamers and (b) fluorescence imaging using the Cy3 fluorescence probe. As shown in Figure 1, the magnetic core was used for cell isolation. Specific cancer cell imaging and separation for the human breast cancer cell line was based on the fact that, in the presence of the SK-BR-3 cell line, S6 aptamer-conjugated magnetic/plasmonic nanoparticles attach to the cancer cells (as shown in Figures 1 and 2) due to the S6 aptamer−cancer cell interaction.

To demonstrate the separation capability of different cancer cells even at 0.01% mixtures, we incubated

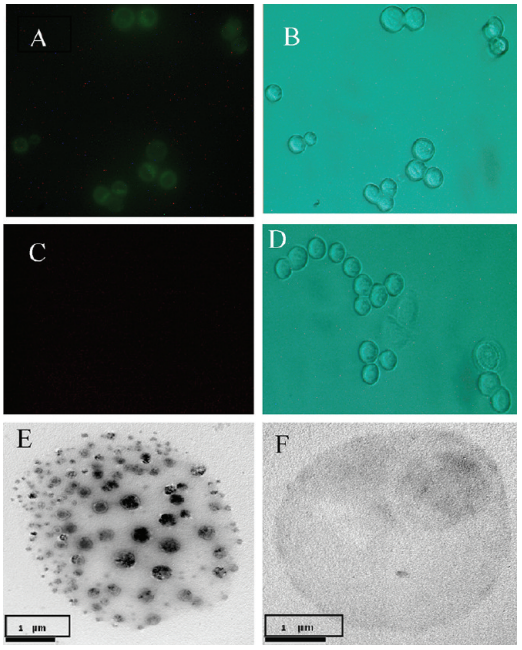

Figure 2. (A) Fluorescent images of SK-BR-3 cancer cells after a mixture of LNCaP and SK-BR-3 cells (1:10^{-4} ratio) was incubated with Cy3-modified S6 aptamer-conjugated magnetic/plasmonic nanoparticles and separated by a magnet. (B) Bright-field image of the same SK-BR-3 cells after magnetic separation. (C) LNCaP cancer cell fluorescent images after a mixture of LNCaP and SK-BR-3 cells (1:10^{-4}) was incubated with Cy3-modified S6 aptamer-conjugated magnetic/plasmonic nanoparticles and separated by a magnet. (D) Bright-field image of the same LNCaP cells after magnetic separation. (E) TEM image of SK-BR-3 cells after magnetic separation. The image clearly shows that Cy3-modified S6 aptamer-conjugated magnetic/plasmonic nanoparticles are attached to SK-BR-3 cells. (F) TEM image of LNCaP cells separated by a magnet.

100 μL of S6 aptamer-conjugated magnetic/plasmonic nanoparticles with 1 mL of HER2-positive human SK-BR-3 breast cancer cell suspension containing 10^3 cells/mL and 1 mL of HER2-negative LNCaP cell suspension containing 10^7 cells/mL. After 120 min incubation at room temperature under gentle shaking, we washed the suspension three times to remove unconjugated Cy3-bound nanoparticles. Next, for both cancer cell suspensions, cancer cells were attached to magnetic nanoparticles and separated by a magnet; then, cancer cells that did not bind with magnetic/plasmonic nanoparticles and were not separated by magnet were characterized using TEM and enzyme-linked immunosorbent assay kits. Cancer cells separated by magnet were also used for fluorescence imaging, as shown in Figure 2. Using enzyme-linked immunosorbent assays, we found no HER2 in the fractions of cell suspensions that did not bind to magnetic/plasmonic nanoparticles, whereas PSMA was present; this clearly shows that the cells are in fact human prostate cancer LNCaP cells. On the other hand, HER2 was present in the fractions of the cell suspension that had attached to the magnetic/plasmonic nanoparticles, clearly indicating that the cells were human breast cancer SK-BR-3 cells. As shown in Figure 2A–D, confocal fluorescence imaging showed

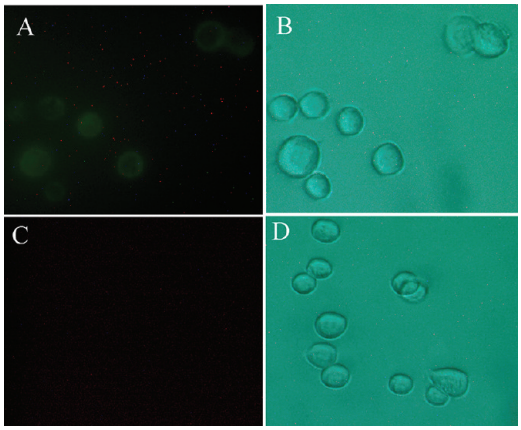

Figure 3. (A) Fluorescent image of SK-BR-3 cancer cells in a mixture of HaCaT and SK-BR-3 cells (1:10^{-5} ratio) incubated with Cy3-modified S6 aptamer magnetic/plasmonic nanoparticles and separated by a magnet. (B) Bright-field image of SK-BR-3 cells after magnetic separation. (C) Fluorescent image of HaCaT cells in a mixture of HaCaT and SK-BR-3 cells (1:10^{-5} ratio) incubated with Cy3-modified S6 aptamer magnetic/plasmonic nanoparticles and separated by a magnet. (D) Bright-field image of MDA-MB cells after magnetic separation.

that the targeted Cy3-bound aptamer-conjugated nanomaterials bound only to SK-BR-3 cells and not HER2-negative LNCaP cells. Similarly, TEM images (Figure 2E,F) indicate that the targeted Cy3-bound aptamer-conjugated nanomaterials bound only to SK-BR-3 cells and not HER2-negative LNCaP cells. Therefore, our results clearly show that S6 aptamer attached to magnetic/plasmonic nanoparticles is highly selective for binding with the SK-BR-3 cell line, which overexpresses HER2; therefore, it can be used for imaging and the separation of different cancer cells even at 0.01% cell mixtures.

As mentioned earlier, it is estimated that, in the early stage of cancer, the concentration of cancer cells is around 0.004% of all white cells in the blood. To demonstrate the separation capability of very low concentrations of cancerous cells (0.001%), we incubated 100 μL of S6 aptamer-conjugated magnetic/plasmonic nanoparticles with 1 mL of HER2-positive human SK-BR-3 breast cancer cell suspension containing 10^2 cells/mL and 1 mL of HER2-negative human skin cell HaCaT cell suspension containing 10^7 cells/mL. After 120 min incubation at room temperature under gentle shaking, we washed the suspension three times to remove unconjugated Cy3-bound magnetic/plasmonic nanoparticles. Then, the cancer cells were separated from the suspension using a small magnet. Using the enzyme-linked immunosorbent assay, we found that there was no HER2 in the portion of the cell suspension that did not bind to magnetic/plasmonic nanoparticles. As discussed earlier, before adding the nanoparticles, we used an enzyme-linked immunosorbent assay kit to determine the amount of HER2 in SK-BR-3 cells and HaCaT cells. Our results show that the amount of HER2 in the SK-BR-3 cells was 6.3 $\times$ 10^6/cell, whereas no

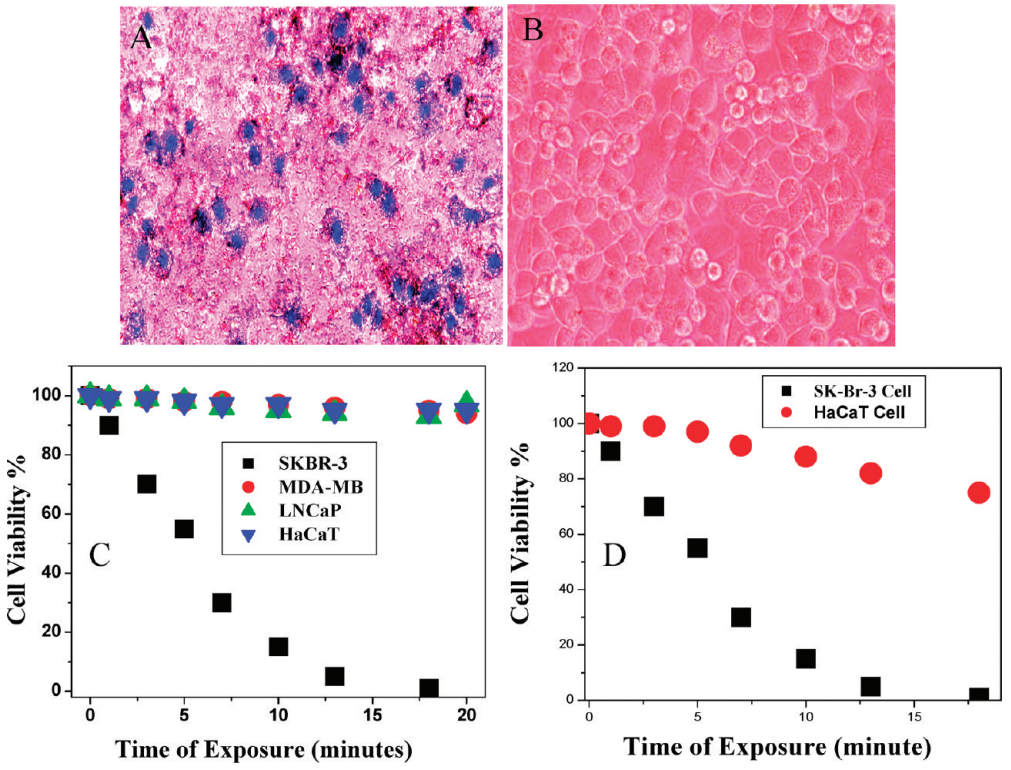

Figure 4. (A) Bright-field inverted microscopic images of aptamer-conjugated magnetic/plasmonic nanoparticles attached to SK-BR-3 breast cancer cells after irradiation with 670 nm light at 2.5 W/cm^2 for 7 min followed by staining with trypan blue. (B) Bright-field inverted microscopic images of SK-BR-3 cells alone after irradiation with 670 nm light at 2.5 W/cm^2 for 10 min followed by staining with trypan blue. (C) Plot showing cell viability when S-6 aptamer-conjugated magnetic/plasmonic nanoparticles attached to SK-BR-3, MDA-MB, and HaCaT cells were treated using 670 nm light at 2.5 W/cm^2 for 20 min. (D) Plot showing cell viability when S-6 aptamer-conjugated magnetic/plasmonic nanoparticles attached to SK-BR-3 and HaCaT cell mixtures (1:0.01) were treated 670 nm light at 2.5 W/cm^2 for 20 min.

HER2 was found in normal HaCaT skin cells. After magnetic separation, we found that there was no HER2 in the portion of the cell suspension that did not bind to magnetic/plasmonic nanoparticles, clearly indicating that it contains HER2-negative HaCaT cells.

As shown in Figure 3, confocal fluorescence imaging also showed that the targeted Cy3-bound aptamer-conjugated nanoparticles bound mostly to the SK-BR-3 cells and did not bind effectively to HER2-negative HaCaT cells. Therefore, the results clearly show that S6 aptamer-bound magnetic/plasmonic nanoparticles highly selectively bind to SK-BR-3 cells overexpressing HER2. Therefore, they can be used for the imaging and separation of breast cancer cells from normal cells even at 0.001% mixtures.

After successful targeted sensing and separation, we performed NIR irradiation experiments to determine whether magnetic/plasmonic nanoparticles can be used for photothermal therapy for SK-BR-3 cancer cells selectively through a gold shell. Initially, the photothermal experiments were performed for each cell line separately in the presence of S6-modified magnetic/plasmonic nanoparticles. Then, we performed the same photothermal experiments for cell mixtures to determine whether this photothermal process is highly selective for cell mixtures. Gold nanoparticles are known to be capable of converting NIR to vibrational energy, generating sufficient heat to kill cancer cells.[8−17,45−64]

In the photothermal destruction experiment, we used 670 nm red light at 2−3 W/cm^2 for 10 min using a 670 nm OEM laser. Since biological systems mostly lack chromophores that absorb in the NIR light range of 650−900 nm, 670 nm is particularly useful in therapy for the induction of hyperthermia. When S6-modified magnetic/plasmonic nanoparticles bound to SK-BR-3 cells are excited with 670 nm light, due to the strong absorption at this wavelength, photoexcitation of the electron gas will result in rapid non-equilibrium heating.

As reported previously,[12,16,49] the initial electronic excitation followed by relaxation will give rise to a rapid increase in the surface temperature of the metal. This initial rapid heating will be cooled to equilibrium by energy exchange between the electrons and lattice. In the first several hundred picoseconds following excitation, the lattice will cool *via* phonons, resulting in local heating surrounding the nanostructure.[12,16,49] This local temperature increase produces sufficient heat for the destruction of magnetic/plasmonic nanoparticles to the SK-BR-3 cancer cells.

To determine the amount of cell death due to this procedure, we added trypan blue after NIR radiation exposure. Living cells cannot bind with trypan blue and

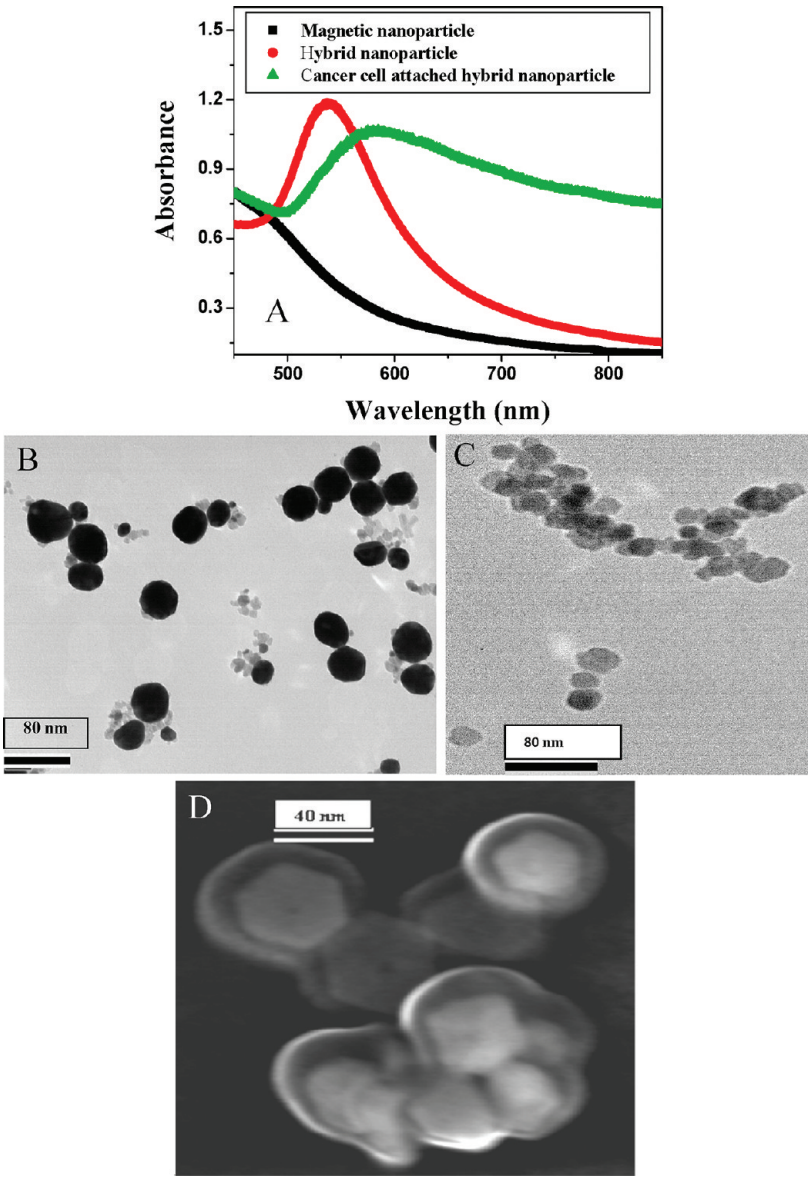

Figure 5. (A) Absorption spectra of SK-BR-3 cancer cells conjugated with magnetic iron oxide (Fe_3O_4) nanoparticles, magnetic core–gold shell nanoparticles, and S6 aptamer-bound magnetic core–gold shell nanoparticles after magnetic separation. (B) TEM image of freshly prepared magnetic nanoparticles. (C) TEM image of freshly prepared plasmonic/magnetic nanoparticles. (D) SEM image of freshly prepared plasmonic/magnetic nanoparticles.

are therefore colorless. On the other hand, dead cells bind with the blue dye. Therefore, cell viability can be qualitatively determined from the color of the cell monolayer. As shown in Figure 4A, most of the cancer cells were dead after 7 min of the nanotherapy process. Bright-field inverted microscope images show that cancer cells were deformed during the nanotherapy process. The cell death following nanoparticle exposure to NIR radiation could be due to numerous factors including nanoparticle explosion, shock waves, bubble formation, and thermal disintegration.[8–17,45–64] Next, to demonstrate that photothermal destruction is highly selective, we performed the same photothermal experiment with HER2-negative MDA-MB breast cancer cells, LNCaP prostate cancer cells, and normal HaCaT cells after incubation with S6 aptamer-conjugated plasmonic/magnetic nanoparticles. All cells were treated using 670 nm light at 2.5 W/cm^2 for 20 min. After that, we used the MTT test to determine the number of live cells after photothermal destruction process. As shown in Figure 4C, the time interval cell viability test indicated that, within 10 min, most of the SK-BR-3 cancer cells were killed. On the other hand, cell viability was more than 93% in the MDA-MB and LNCaP cells and 96% for the HaCaT cells. This is because the conjugation of magnetic/plasmonic nanoparticles with cancer cells is necessary for photothermal destruction using 670 nm light. Cancer cells conjugated with magnetic/plasmonic nanoparticles should have strong absorption at the excitation wavelength, which is 670 nm in our case. As shown in Figures 2 and 3, the conjugation of magnetic/plasmonic nanoparticles on cell membranes occurred only in HER2-positive SK-BR-3 cells.

Therefore, the photothermal destruction effect should be highly efficient in the presence of SK-BR-3 cells compared to MDA-MB, LNCaP, or HaCaT cells. As shown in Figure 5C, since the magnetic/plasmonic nanoparticle-conjugated SK-BR-3 cancer cells absorb 670 nm light, the presence of such light will generate heat, which will destroy the SK-BR-3 cells. On the other hand, due to the lack of conjugation between magnetic/plasmonic nanoparticles and MDA-MB or LNCaP or HaCaT cells, combinations of magnetic/plasmonic nanoparticles and any of these cells do not have enough absorption at 670 nm. Therefore, during photothermal destruction using 670 nm light, the effective temperature increase in cancer cells will be very little, which will be insufficient to kill these cells. Next, to understand how temperature increases during photothermal destruction, we performed thermal imaging at 1 min intervals during the therapy process using a Mikro-Shot camera. We found that the temperature increased to about 55 °C when exposing magnetic/plasmonic nanoparticle-bound cancer cells to a 670 nm laser at 2.5 W/cm^2. On the other hand, in the same condition, the temperature increased to only 35 °C for MDA-MB and LNCaP cancer cells without any nanoparticles.

In clinical situations, cancer cells are always surrounded by healthy normal cells. Once we found that S6 aptamer-attached magnetic core–plasmonic shell nanoparticles can be used to selectively kill SK-BR-3 cell, we determined whether selective photothermal destruction can be performed in mixtures of cells. For this purpose, we used a HaCaT and SK-BR-3 cell mixture (1:1) incubated with S6 aptamer-conjugated magnetic/plasmonic nanoparticles for 2 h. Then, the cell mixtures were treated using 670 nm light at 2.5 W/cm^2 for up to 20 min. Next, we separated the cells using magnets and used the MTT test to determine the percentages of live cells during the photothermal destruction process. As shown in Figure 4D, normal cells started to die after 6 min of therapy. At 13 min, when about 100% of cancer cells were dead, only 12% of normal cells were dead. As discussed earlier, when we used individual cell lines, the photothermal destruction was highly selective.

On the other hand, in the case of cell mixtures, only 12% of normal cells were killed. This is because, for the photothermal destruction experiment, very small volumes (100 μL) of the sample were exposed to the 670 nm light. As a result, there was an increase in the temperature of the whole suspension during the therapy process. As a result, normal cells were also killed in the mixture even though they were not attached to S6 aptamer-conjugated magnetic/plasmonic nanoparticles. In clinical situations, some heat may dissipate through floating body liquids. Therefore, we may observe a negligible amount of normal cell death. Of course, it is preferable if the photothermal process can finish within 5 min using a slightly more powerful NIR pulsed laser.

CONCLUSIONS

In conclusion, we demonstrated the use of S6 aptamer-conjugated magnetic core–plasmonic shell nanoparticles for the targeted diagnosis, isolation, and photothermal destruction of SK-BR-3 human cancer cells. We also found that bioconjugated magnetic/plasmonic nanoparticles highly selectively bind to SK-BR-3 cells, which overexpress HER2. Experimental data with a mixture of SK-BR-3, HaCaT, or LNCaP prostate cancer cell lines clearly demonstrate that bioconjugated plasmonic/magnetic nanoparticles can be used for imaging and magnetic separation even in 0.001% mixtures. We also demonstrated that, during the photothermal destruction of SK-BR-3 cancerous cells bound to S6 aptamer-conjugated magnetic/plasmonic nanoparticles, the localized heating that occurs due to the absorption of 670 nm continuous NIR irradiation is able to cause irreparable cellular damage; it selectively kills most of the cancerous cells within 10 min at 2.5 W/cm^2. This magnetic core–plasmonic shell nanotechnology-based assay is rapid; it only takes about 30 min from cancer cell binding to isolation and cell destruction. Even though magnetic/plasmonic nanoparticles have demonstrated promising results for cancer imaging, isolation, and therapy, it is only fair to admit that we are at a relatively early stage of development. The photothermal destruction treatment results of cell mixtures demonstrate that small amounts of normal cell death may also occur during photothermal destruction. Depending on how fast heat may dissipate through floating body liquids and how fast we can finish the photothermal destruction process, some healthy cell death may occur during the photothermal destruction process in clinical practice. After the optimization of different parameters, we believe that this hybrid nanotechnology-driven assay could have enormous potential for applications in the rapid detection and photothermal destruction of clinical samples.

METHODS

Materials. Hydrogen tetrachloroaurate ($HAuCl_4 \cdot 3H_2O$), $NaBH_4$, sodium citrate, and iron chloride were purchased from Sigma-Aldrich, USA, and used without further purification. The human breast cancer and prostate cancer cell lines were purchased from the American Type Culture Collection (ATCC, Rockville, MD). The human skin HaCaT keratinocyte cell line, a transformed human epidermal cell line, was obtained from Dr. Norbert Fusenig of the Germany Cancer Research Center.

Synthesis of Magnetic Core–Gold Shell Gold Nanoparticles. Magnetic core nanoparticles were synthesized by co-precipitation of Fe(II) and Fe(III) chlorides with 1.5 M NaOH as a reductant as described previously.[35,36] At the end of the procedure, the black precipitate was collected on a magnet and washed several times

with water and tetramethylammonium hydroxide (TMAOH). Gold shells were formed by the reduction of Au^{3+} onto the iron oxide surfaces as shown in Figure 1. We initially dissolved 30 mg of iron oxide nanoparticles in 30 mL of water and heated it until boiling. Then, we added 5 mL of 10^{-2} M gold chloride solution, followed by the addition of trisodium citrate. Then, we boiled the solution for another 15–20 min; this step was repeated three times to make thick gold shells. The final solution appeared light pink brown in color. A JEM-2100F TEM and UV–visible absorption spectrum were used to characterize the nanoparticles (Figure 5).

Synthesis of Aptamer-Conjugated Magnetic/Plasmonic Nanoparticles. Thiol-modified Cy3-bound S6 aptamers were gradually exposed to magnetic core–plasmonic shell nanoparticles in the presence of 0.1 M NaCl in a PBS buffer over a 16 h period. To remove the unbound aptamers, we centrifuged the solution at 6000 rpm for 20 min, and the precipitate was then redispersed in 2 mL of buffer solution; we repeated this process three times. To measure the number of aptamer molecules in each plasmonic/magnetic nanoparticle, we performed fluorescence analyses after the addition of potassium cyanide. To measure the number of aptamer molecules in each gold nanoparticle, after conjugation, we treated the Cy3-bound S6 aptamer-conjugated gold nanoparticles with 10 μM potassium cyanide to oxidize them. After that, the solution containing the released Cy3-labeled aptamers was collected for fluorescence analysis.

The amount of Cy3-labeled S6 aptamers was measured by fluorescence. By dividing the total number of Cy3-labeled S6 aptamers by the total number of nanoparticles, we estimated that there were about 100–140 aptamers per magnetic/plasmonic nanoparticle. To characterize the hybrid nanoparticle conjugates according to S6 aptamer size, we performed DLS measurements. The experimental data show that the overall particle diameter was around 55 ± 3 nm, which is a good size for the development of theranostic agents as reported recently.[70]

Cell Culture and Incubation with Magnetic/Plasmonic Nanoparticles. Cancer cells were grown in a 5% CO_2 incubator at 37 °C using RPMI-1640 medium (ATCC, Rockville, MD) supplemented with 10% premium fetal bovine serum (FBS) (Lonza, Walkersville, MD) and antibiotics (10 IU/mL penicillin G and streptomycin) in 75 cm^2 tissue culture flasks. An enzyme-linked immunosorbent assay kit was used to quantify HER2 in tested cells. The experimental results indicate that the amount of HER2 in SK-BR-3 cells was 6.3×10^6/cell but only 1.1×10^3/cell in MDA-MB breast cancer cells. No HER2 was observed in the LNCaP and HaCaT cell lines. Different numbers of cells were then immersed into the aptamer-conjugated magnetic/plasmonic nanoparticle solution at room temperature before performing the magnetic separation experiment. After magnetic separation, we performed TEM and fluorescence analyses (Figure 2). The absorption data show that SK-BR-3 cells bound to magnetic–plasmonic nanoparticles have quite broad absorption (Figure 5); this may be due to the aggregation of nanoparticles on SK-BR-3 cancer cell surfaces as shown in the TEM picture in Figure 2F.

Fluorescence Analysis. After cell separation by magnet, we used an Olympus IX71 inverted confocal fluorescence microscope fitted with a SPOT Insight digital camera for fluorescence imaging.

Photothermal Destruction and Determination of the Percentage of Live Cells. For the photothermal destruction experiments, we used a continuous-wavelength portable OEM laser operating at 670 nm as an excitation light source for 10–20 min. Then, we used the MTT test to determine the amounts of live cells after the photothermal destruction process. For this purpose, prostate cancer cells were seeded in 96-well plates (well diameter, 6.4 mm) at a density of 1×10^5 cells/well and were allowed to attach for 24 h at 37 °C in a 5% CO_2 incubator before the treatment. The cell monolayers in the wells were repeatedly rinsed with PBS buffer after incubation to remove the nonspecifically adsorbed nanomaterial remaining in the medium. Then, the monolayers were exposed to the 670 nm laser. Cell viability was also determined 1 h after photothermal treatment using the 3-(4,5-dimethylthiazol-2-yl)-2,5-diphenyltetrazolium bromide (MTT) cell proliferation assay kit (ATCC CA# 30-1010k). This experiment was repeated 5–6 times. The results are expressed as mean values.

Conflict of Interest: The authors declare no competing financial interest.

Acknowledgment. P.C.R. is grateful for NSF-PREM Grant No. DMR-0611539 for their generous funding for nanomaterial research, NIH-RCMI Grant No. 5G12RR013459 for core facilities, and NIH-MARC Grant No. 5-T34-GM007672-28 from the Melanie Shelton scholarship. We also thank all reviewers for their valuable suggestions, which improved the quality of the manuscript.

REFERENCES AND NOTES

1. Bray, F.; Møller, B. Predicting the Future Burden of Cancer. *Nat. Rev. Cancer* **2006**, *6*, 63–74.
2. World Health Organization; http://www.who.int/cancer/en (accessed July 9, 2011).
3. National Cancer Institute; http://www.cancer.gov/cancertopics/types/breast (accessed July 9, 2011).
4. National Cancer Institute; http://www.cancer.gov/cancertopics/types/prostate (accessed July 9, 2011).
5. Centers for Disease Control and Prevention; http://www.cdc.gov/cancer/nbccedp (accessed July 9, 2011).
6. Chen, H. Z.; Tsai, S. Y.; Leone, G. Emerging Roles of E2FS in Cancer: An Exit from Cell Cycle Control. *Nat. Rev. Cancer* **2009**, *9*, 785–797.
7. Sarkar, B.; Dosch, J.; Simeone, D. M. Cancer Stem Cells: A New Theory Regarding a Timeless Disease. *Chem. Rev.* **2009**, *109*, 3200–3208.
8. Lu, W.; Singh, A. K.; Khan, S. A.; Senapati, D.; Yu, H.; Ray, P. C. Gold Nano-Popcorn-Based Targeted Diagnosis, Nanotherapy Treatment, and *In Situ* Monitoring of Photothermal Destruction Response of Prostate Cancer Cells Using Surface-Enhanced Raman Spectroscopy. *J. Am. Chem. Soc.* **2010**, *132*, 18103–18114.
9. Ljungman, M. Targeting the DNA Damage Response in Cancer. *Chem. Rev.* **2009**, *109*, 2929–2950.
10. Ferrari, M. Cancer Nanotechnology: Opportunities and Challenges. *Nat. Rev. Cancer* **2005**, *5*, 161–171.
11. Scheinberg, D. A.; Villa, C. H.; Escorcia, F. E.; McDevitt, R. M. Conscripts of the Infinite Armada: Systemic Cancer Therapy Using Nanomaterials. *Nat. Rev. Clin. Oncol.* **2010**, *7*, 266–276.
12. Jain, P. K.; Huang, X.; El-Sayed, I. H.; El-Sayed, M. A. Noble Metals on the Nanoscale: Optical and Photothermal Properties and Some Applications in Imaging, Sensing, Biology, and Medicine. Noble Metals on the Nanoscale: Optical and Photothermal Properties and Some Applications in Imaging, Sensing, Biology, and Medicine. *Acc. Chem. Res.* **2008**, *41*, 1578–1586.
13. King, S. H.; Huh, Y. M.; Kim, S.; Lee, D.-K. Isolation of RNA Aptamers Targeting HER-2-Overexpressing Breast Cancer Cells Using Cell-SELEX. *Bull. Korean Chem. Soc.* **2009**, *30*, 1827–1831.
14. Fang, X.; Tan, W. Aptamers Generated from Cell-SELEX for Molecular Medicine: A Chemical Biology Approach. *Acc. Chem. Res.* **2010**, *43*, 48–57.
15. Famulok, M.; Hartig, J. S.; Mayer, M. Functional Aptamers and Aptazymes in Biotechnology, Diagnostics, and Therapy. *Chem. Rev.* **2007**, *107*, 3715–3743.
16. Lal, S.; Clare, S. E.; Halas, N. J. Nanoshell-Enabled Photothermal Cancer Therapy: Impending Clinical Impact. *Acc. Chem. Res.* **2008**, *41*, 1842–1851.
17. Bardhan, R.; Lal, S.; Joshi, A.; Halas, N. J. Theranostic Nanoshells: From Probe Design to Imaging and Treatment of Cancer. *Acc. Chem. Res.* **2011**, *44*, 936–946.
18. Gao, J.; Gu, H.; Xu, B. Multifunctional Magnetic Nanoparticles: Design, Synthesis, and Biomedical Applications. *Acc. Chem. Res.* **2009**, *42*, 1097–1107.
19. Xie, J.; Liu, G.; Eden, H. S.; Ai, H.; Chenm, X. Surface-Engineered Magnetic Nanoparticle Platforms for Cancer Imaging and Therapy. *Acc. Chem. Res.* **2011**, *44*, 883–892.
20. Tassa, C.; Shaw, S. Y.; Weissleder, R. Dextran-Coated Iron Oxide Nanoparticles: A Versatile Platform for Targeted Molecular Imaging, Molecular Diagnostics, and Therapy. *Acc. Chem. Res.* **2011**, *44*, 842–852.
21. Kievit, F. M.; Zhang, M. Surface Engineering of Iron Oxide Nanoparticles for Targeted Cancer Therapy. *Acc. Chem. Res.* **2011**, *44*, 853–862.

22. Peer, D.; Karp, J. M.; Hong, S.; Farokhzad, O. C.; Margalit, R.; Langer, R. Nanocarriers as an Emerging Platform for Cancer Therapy. *Nat. Nanotechnol.* **2007**, *2*, 751–760.
23. Giljohann, D. A.; Mirkin, C. A. Drivers of Biodiagnostic Development. *Nature* **2009**, *462*, 461–464.
24. Sun, C.; Du, K.; Fang, C.; Bhattarai, N.; Veiseh, O.; Kievit, F.; Stephen, Z.; Lee, D.; Ellenbogen, R. G.; Ratner, B. PEG-Mediated Synthesis of Highly Dispersive Multifunctional Superparamagnetic Nanoparticles: Their Physicochemical Properties and Function *in Vivo*. *ACS Nano* **2010**, *4*, 2402–2410.
25. Kim, B.; Han, G.; Toley, B. J.; Kim, C. K.; Rotello, V. M.; Forbes, N. S. Tuning Payload Delivery in Tumour Cylindroids Using Gold Nanoparticles. *Nat. Nanotechnol.* **2010**, *5*, 465–472.
26. Kievit, F. M.; Veiseh, O.; Fang, C.; Bhattarai, N.; Lee, D.; Ellenbogen, R. G.; Zhang, M. Chlorotoxin-Labeled Magnetic Nanovectors for Targeted Gene Delivery to Glioma. *ACS Nano* **2010**, *4*, 4587–4594.
27. Thomas, C. R.; Ferris, D. P.; Lee, J. H.; Choi, E.; Cho, M. H.; Kim, E. S.; Stoddart, J. F.; Shin, J. S.; Cheon, J.; Zink, J. I. Noninvasive Remote-Controlled Release of Drug Molecules *in Vitro* Using Magnetic Actuation of Mechanized Nanoparticles. *J. Am. Chem. Soc.* **2010**, *132*, 10623–10625.
28. Ruiz-Hernández, E.; Baeza, A.; Vallet-Reg, M. Smart Drug Delivery through DNA/Magnetic Nanoparticle Gates. *ACS Nano* **2011**, *5*, 1259–1266.
29. Meledandri, C. J.; Stolarczyk, J. K.; Brougham, D. F. Hierarchical Gold-Decorated Magnetic Nanoparticle Clusters with Controlled Size. *ACS Nano* **2011**, *5*, 1747–1755.
30. Lee, J.-H.; Huh, Y.-M.; Jun, Y.-W.; Seo, J.-W.; Jang, J.-T.; Song, H.-T.; Kim, S.; Cho, E.-J.; Yoon, H.-G.; Suh, J.-S. Artificially Engineered Magnetic Nanoparticles for Ultrasensitive Molecular Imaging. *Nat. Med.* **2007**, *13*, 95–99.
31. Barnett, B. P.; Arepally, A.; Karmarkar, P. V.; Qian, D.; Gilson, W. D.; Walczak, P.; Howland, V.; Lawler, L.; Lauzon, C.; Stuber, M.; *et al.* Magnetic Resonance-Guided, Real-Time Targeted Delivery and Imaging of Magnetocapsules Immunoprotecting Pancreatic Islet Cells. *Nat. Med.* **2007**, *13*, 986–991.
32. Bruns, O. T.; Ittrich, H.; Peldschus, K.; Kaul, M. G.; Tromsdorf, U. I.; Lauterwasser, J.; Nikolic, M. S.; Mollwitz, B.; Merkel, M.; Bigall, N. C.; *et al.* Real-Time Magnetic Resonance Imaging and Quantification of Lipoprotein Metabolism *in Vivo* Using Nanocrystals. *Nat. Nanotechnol.* **2009**, *4*, 193–201.
33. Levin, C. S.; Hoffman, C.; Ali, T. A.; Kelly, A. T.; Morosan, E.; Nordlander, P.; Whitmire, K. H.; Halas, N. J. Magnetic–Plasmonic Core–Shell Nanoparticles. *ACS Nano* **2009**, *3*, 1379–1388.
34. Zhang, Q.; Ge, J.; Goebl, J.; Hu, Y.; Sun, Y.; Yin, Y. Tailored Synthesis of Superparamagnetic Gold Nanoshells with Tunable Optical Properties. *Adv. Mater.* **2010**, *22*, 1905–1909.
35. Lyon, J. L.; Fleming, D. A.; Stone, M. B.; Schiffer, P.; Williams, M. E. Synthesis of Fe Oxide Core/Au Shell Nanoparticles by Iterative Hydroxylamine Seeding. *Nano Lett.* **2004**, *4*, 719–723.
36. Laurent, S.; Forge, D.; Port, M.; Roch, A.; Robic, C.; Vander Elst, L.; Muller, R. N. Magnetic Iron Oxide Nanoparticles: Synthesis, Stabilization, Vectorization, Physicochemical Characterizations, and Biological Applications. *Chem. Rev.* **2008**, *108*, 2064–2110.
37. Song, E.-Q.; Hu, J.; Wen, C.-Y.; Tian, Z.-Q.; Yu, X.; Zhang, Z.-L.; Shi, Y. B.; Pang, D. W. Fluorescent-Magnetic-Biotargeting Multifunctional Nanobioprobes for Detecting and Isolating Multiple Types of Tumor Cells. *ACS Nano* **2011**, *5*, 761–770.
38. Schuller, J. A.; Barnard, E. S.; Ca, W. I.; Jun, Y. C.; White, J. S.; Brongersma, M. L. Plasmonics for Extreme Light Concentration and Manipulation. *Nat. Mater.* **2010**, *9*, 193–204.
39. Yong, K.-T.; Ding, H.; Roy, I.; Law, W.-C.; Bergey, E. J.; Maitra, A.; Prasad, P. N. Imaging Pancreatic Cancer Using Bioconjugated InP Quantum Dots. *ACS Nano* **2009**, *3*, 502–510.
40. Bhirde, A. A.; Patel, V.; Gavard, J.; Zhang, G.; Sousa, A. A.; Masedunskas, A.; Leapman, R. D.; Weigert, R.; Gutkind, S. J.; Rusling, J. F. Targeted Killing of Cancer Cells *in Vivo* and *in Vitro* with EGF-Directed Carbon Nanotube-Based Drug Delivery. *ACS Nano* **2009**, *3*, 307–316.
41. Fang, Z.; Soleymani, L.; Pampalakis, G.; Yoshimoto, M.; Squire, J. A.; Sargent, E. H.; Kelley, S. O. Direct Profiling of Cancer Biomarkers in Tumor Tissue Using a Multiplexed Nanostructured Microelectrode Integrated Circuit. *ACS Nano* **2009**, *3*, 3207–3213.
42. Erogbogbo, F.; Yong, K.-T.; Roy, I.; Xu, G.; Prasad, P. N.; Swihart, M. T. Biocompatible Luminescent Silicon Quantum Dots for Imaging of Cancer Cells. *ACS Nano* **2008**, *2*, 873–878.
43. Kumar, R.; Roy, I.; Ohulchanskky, T. Y.; Vathy, L. A.; Bergey, E. J.; Sajjad, M.; Prasad, P. N. *In Vivo* Biodistribution and Clearance Studies Using Multimodal Organically Modified Silica Nanoparticles. *ACS Nano* **2010**, *4*, 699–708.
44. Yezhelyev, M. V.; Al-Hajj, A.; Morris, C.; Marcus, A. I.; Liu, T.; Lewis, M.; Cohen, C.; Zrazhevskiy, P.; Simons, J. W.; Rogatko, A.; *et al.* *In Situ* Molecular Profiling of Breast Cancer Biomarkers with Multicolor Quantum Dots. *Adv. Mater.* **2007**, *19*, 3146–3151.
45. Bhaskara, V. C.; Vyomesh, P.; Silvio, G. J.; James, F. R. Ultrasensitive Immunosensor for Cancer Biomarker Proteins Using Gold Nanoparticle Film Electrodes and Multienzyme-Particle Amplification. *ACS Nano* **2009**, *3*, 585–594.
46. Liu, X.; Dai, Q.; Austin, L.; Coutts, J.; Knowles, G.; Zou, J.; Chen, H.; Huo, Q. A One-Step Homogeneous Immunoassay for Cancer Biomarker Detection Using Gold Nanoparticle Probes Coupled with Dynamic Light Scattering. *J. Am. Chem. Soc.* **2008**, *130*, 2780–2782.
47. Li, S. J.; Li, J.; Wang, K.; Wang, C.; Xu, J.-J.; Chen, H.-Y.; Xia, X.-H.; Huo, Q. A Nanochannel Array-Based Electrochemical Device for Quantitative Label-Free DNA Analysis. *ACS Nano* **2010**, *4*, 6417–6424.
48. Moon, H. K.; Lee, S. H.; Choi, H. C. *In Vivo* Near-Infrared Mediated Tumor Destruction by Photothermal Effect of Carbon Nanotubes. *ACS Nano* **2009**, *3*, 3707–3713.
49. Huang, X.; El-Sayed, I. H.; Qian, W.; El-Sayed, M. A. Cancer Cell Imaging and Photothermal Therapy in the Near-Infrared Region by Using Gold Nanorods. *J. Am. Chem. Soc.* **2006**, *128*, 2115–2120.
50. Lu, W.; Arumugam, S. R.; Senapati, D.; Singh, A. K.; Arbneshi, T.; Khan, S. A.; Yu, H.; Ray, P. C. Multifunctional Oval Shape Gold Nanoparticle Based Selective Detection of Breast Cancer Cells Using Simple Colorimetric and Highly Sensitive Two-Photon Scattering Assay. *ACS Nano* **2010**, *4*, 1739–1749.
51. Wijaya, A.; Schaffer, S. B.; Pallares, I. G.; Hamad-Schifferli, K. Selective Release of Multiple DNA Oligonucleotides from Gold Nanorods. *ACS Nano* **2009**, *3*, 80–86.
52. Braun, G. B.; Pallaoro, A.; Wu, G.; Missirlis, D.; Zasadzinski, J. A.; Tirrell, M.; Reich, N. O. Laser-Activated Gene Silencing *via* Gold Nanoshell–siRNA Conjugates. *ACS Nano* **2009**, *3*, 2007–2015.
53. Ray, P. C. Size and Shape Dependent Second Order Nonlinear Optical Properties of Nanomaterials and Their Application in Biological and Chemical Sensing. *Chem. Rev.* **2010**, *110*, 5332–5365.
54. Neely, A.; Perry, C.; Varisli, B.; Singh, A. K.; Arbneshi, T.; Senapati, D.; Kalluri, J. R.; Ray, P. C. Ultrasensitive and Highly Selective Detection of Alzheimer's Disease Biomarker Using Two-Photon Rayleigh Scattering Properties of Gold Nanoparticle. *ACS Nano* **2009**, *3*, 2834–2840.
55. Singh, A. K.; Senapati, D.; Wang, S.; Griffin, J.; Neely, A.; Candice, P.; Naylor, K. M.; Varisli, B.; Kalluri, J. R.; Ray, P. C. Gold Nanorod Based Selective Identification of *Escherichia coli* Bacteria Using Two-Photon Rayleigh Scattering Spectroscopy. *ACS Nano* **2009**, *3*, 1906–1912.
56. Griffin, J.; Singh, A. K.; Senapati, D.; Lee, E.; Gaylor, K.; Boone, J. J.; Ray, P. C. Sequence Specific HCV-RNA Quantification Using Size Dependent Nonlinear Optical Properties of Gold Nanoparticles. *Small* **2009**, *5*, 839–845.
57. Griffin, J.; Singh, A. K.; Senapati, D.; Rhodes, P.; Mitchell, K.; Robinson, B.; Yu, E.; Ray, P. C. Size and Distance Dependent NSET Ruler for Selective Sensing of Hepatitis C Virus RNA. *Chem.—Eur. J.* **2009**, *15*, 342–351.
58. Darbha, G. K.; Rai, U. S.; Singh, A. K.; Ray, P. C. Highly Selective Detection of Hg^{2+} Ion Using NLO Properties of

Gold Nanomaterial. *J. Am. Chem. Soc.* **2008**, *130*, 8038–8042.
59. Darbha, G. K.; Rai, U. S.; Singh, A. K.; Ray, P. C. Gold Nanorod Based Sensing of Sequence Specific HIV-1 Virus DNA Using Hyper Rayleigh Scattering Spectroscopy. *Chem.—Eur. J.* **2008**, *14*, 3896–3903.
60. Darbha, G. K.; Ray, A.; Ray, P. C. Gold Nanoparticle-Based Miniaturized FRET Probe for Rapid and Ultrasensitive Detection of Mercury in Soil, Water, and Fish. *ACS Nano* **2007**, *3*, 208–214.
61. Wang, S.; Singh, A. K.; Senapati, D.; Neely, A.; Yu, H.; Ray, P. C. Rapid Colorimetric Identification and Targeted Photothermal Lysis of *Salmonella* Bacteria by Using Bioconjugated Oval-Shaped Gold Nanoparticles. *Chem.—Eur. J.* **2010**, *16*, 5600–5606.
62. Gobin, A. M.; Watkins, E. M.; Quevedo, E.; Colvin, V.; West, J. L. Near-Infrared-Resonant Gold/Gold Sulfide Nanoparticles as a Photothermal Cancer Therapeutic Agent. *Small* **2010**, *6*, 745–752.
63. Bae, K. H.; Kim, Y. B.; Lee, Y.; Hwang, J. Y.; Park, H. W.; Park, T. G. Bio-inspired Synthesis and Characterization of Gadolinium-Labeled Magnetite Nanoparticles for Dual Contrast T1- and T2-Weighted Magnetic Resonance Imaging. *Bioconjugate Chem.* **2010**, *21*, 505–512.
64. Singh, A. K.; Lu, W.; Senapati, D.; Khan, S. A.; Fan, Z.; Senapati, T.; Demeritte, T; Beqa, L.; Ray, P. C. Long-Range Nanoparticle Surface-Energy-Transfer Ruler for Monitoring Photothermal Therapy Response. *Small* **2011**, *7*, 2517–2525.
65. Butler, T. P.; Gullino, P. M. Quantitation of Cell Shedding into Efferent Blood of Mammary Adenocarcinoma. *Cancer Res.* **1975**, *35*, 512–516.
66. Liotta, L. A.; Saidel, M. G.; Kleinerman, J. The Significance of Hematogenous Tumor Cell Clumps in the Metastatic Process. *J. Cancer Res.* **1976**, *36*, 889–894.
67. Xu, Y.; Phillips, J. A.; Yan, J.; Li, Q.; Fan, Z. H.; Tan, W. Aptamer-Based Microfluidic Device for Enrichment, Sorting, and Detection of Multiple Cancer Cells. *Anal. Chem.* **2009**, *81*, 7436–7442.
68. Zborowski, M.; Chalmers, J. J. Rare Cell Separation and Analysis by Magnetic Sorting. *Anal. Chem.* **2011**, *83*, 8050–8056.
69. Huang, Y. F.; Sefah, K.; Bamrungsap, S.; Chang, H. T.; Tan, W. Selective Photothermal Therapy for Mixed Cancer Cells Using Aptamer-Conjugated Nanorods. *Langmuir* **2008**, *24*, 11860–11865.
70. Ma, L. L.; Tam, J. O.; Willsey, B. W.; Rigdon, D.; Ramesh, R.; Sokolov, S.; Johnston, K. P. Selective Targeting of Antibody Conjugated Multifunctional Nanoclusters (Nanoroses) to Epidermal Growth Factor Receptors in Cancer Cells. *Langmuir* **2011**, *27*, 7681–7690.